Mon. Not. R. Astron. Soc. **343,** 1123–1130 (2003)

Frictional and radiation heating of micron-sized meteoroids in the Earth's upper atmosphere

S. G. Coulson[1]★ and N. C. Wickramasinghe[2]

[1]*School of Mathematics, Cardiff University, PO Box 926, Senghennydd Road, Cardiff CF2 4YH*
[2]*Cardiff Centre for Astrobiology, Cardiff University, 2 North Road, Cardiff CF10 3DY*

Accepted 2003 January 30. Received 2003 January 27; in original form 2002 August 8

ABSTRACT

This paper follows on from earlier work presented on the dynamics of micron-sized meteoroid particles, as they are decelerated in the Earth's atmosphere at heights of 100 km or greater. Here the heating effects on these meteoroids are examined; both the intense heating during deceleration and the temperatures reached by particles settling through the atmosphere with low speeds ∼cm s^{-1} are considered. Meteoroid deceleration by sputtering of molecules from the surface is shown to provide a mechanism by which small particles can decelerate from high entry speeds down to speeds of the order of cm s^{-1} while avoiding extreme heating. The question of survivability of organic material on meteoroid bodies in free space and during descent through the Earth's atmosphere is addressed.

Key words: astrobiology – meteors, meteoroids – ISM: kinematics and dynamics.

1 INTRODUCTION

Earlier work (Coulson 2002) has examined the dynamics of small meteoroids as they descend through the upper portion of the Earth's atmosphere. Equations of motion were derived taking into account the resistance to motion for spherical particles passing through a low-density gas, conditions similar to those at altitudes 90 km or greater above the surface of the Earth. In this paper, the effects of frictional heating from the air molecules impinging on a meteoroid, together with radiation absorbed by the meteoroid from both the atmosphere and the Sun, are considered. Analytical and semi-analytical models to determine particle temperature as a function of altitude above the Earth's surface are derived. Models for a range of particle parameters are developed.

The problem of meteoroids being heated as they pass through the atmosphere has been studied for a range of meteoroid sizes (Whipple 1950; Bronshten 1983). Work on the heating of micrometeoroids with radii from 10 μm to 0.1 cm has been carried out by Love & Brownlee (1991). These authors restricted themselves to a minimum particle radius of 10 μm; for particles smaller than this, radiation scattering complicates the issue. The problem of micron-sized meteoroids is of interest because of the question of survivability of organic and pre-biotic or biological material as it falls towards the Earth's surface. The majority of the ∼100 tonnes of cometary material incident on the top of the Earth's atmosphere per day is within the size range ∼10 μm to 0.1 cm (Love & Brownlee 1993; Allen 2000), so it is reasonable to assume that the bulk of organic material included in this daily input falls within this size distribution.

★E-mail: Coulsonsg@cf.ac.uk (SGC); Wickramasinghe@cf.ac.uk (NCW)

2 FREE GRAINS AT A SOLAR DISTANCE OF 1 AU

2.1 Heating of micrometeoroids in space

For a dust particle in free space, the only effective mechanism by which it can radiate energy is thermal re-emission at the temperature T_g of the solid lattice. The energy re-emitted per unit time for a spherical particle of radius a is given by

$$4\pi a^2 \int_\lambda \mathrm{d}\lambda\, Q_{\mathrm{abs}}(\lambda, a) B(\lambda, T_g), \tag{2.1.1}$$

where Q_{abs} is the absorption cross-section and B is the Planck function at temperature T_g.

Within the Solar system the main source of heating of interplanetary bodies such as asteroids and cometary fragments in free space comes from the Sun. The radiation absorbed by a spherical particle of radius a, per unit time, is

$$W\pi a^2 \int_\lambda \mathrm{d}\lambda\, Q_{\mathrm{abs}}(\lambda, a) B(\lambda, T_\odot). \tag{2.1.2}$$

Equation (2.1.2) assumes that the radiation field from the Sun can be approximated as a blackbody, with a Planck spectrum at an effective solar temperature $T_0 \sim 6000$ K. The use of the absorption coefficient for the emissivity is guaranteed by considerations of time reversal symmetry (Bohren & Huffman 1983). W is the dilution factor for the radiation field and is proportional to the inverse square of the distance of the particle from the Sun. At 1 au, $W \approx 2.15 \times 10^{-5}$.

For a grain in thermal equilibrium, the balance equation can be written as

$$W\int_{\lambda} \mathrm{d}\lambda Q_{\mathrm{abs}}(\lambda, a)B(\lambda, T_{\odot}) = 4\int_{\lambda} \mathrm{d}\lambda Q_{\mathrm{abs}}(\lambda, a)B(\lambda, T_{\mathrm{g}}). \quad (2.1.3)$$

The majority of particles making up interplanetary dust absorb radiation in the visible range and re-emit at infrared wavelengths. For practical purposes the left-hand side of (2.1.3) is normally integrated over near-ultraviolet and visible wavelengths (typically 0.2–0.8 μm) and the right-hand side over those of the infrared (typically 2–12 μm). For a grain at a temperature of 1000 K, re-emission mainly corresponds to a wavelength of ∼3 μm.

For particles of radii comparable to that of the absorbed or emitted radiation, the scattering of the electromagnetic radiation complicates the process. In general there are three distinct cases to consider:

(i) the blackbody limit – particles with radii greater than the wavelengths of the absorbed and emitted radiation, $a \gg 10$ μm;

(ii) the Mie-scattering region – particles with radii comparable to the wavelengths of the absorbed and emitted radiation, $0.01 < a < 10$ μm;

(iii) the asymptotic Rayleigh limit – particles with radii such that $2\pi a \ll \lambda$ at all relevant wavelengths.

2.2 The blackbody limit

In this limit the particle radii are much greater than the radiation wavelengths, which applies for particles with radii of 10 μm or more. In this case the particle can be assumed to be a blackbody, $Q_{\mathrm{abs}} \approx 1$. For such a particle at a distance R from the Sun, the solar flux is given by (Kuhrt 1984)

$$\frac{\pi(1-A)R_{\odot}^2\sigma T_{\mathrm{eff}}^4}{R^2}, \quad (2.2.1)$$

where A is the albedo, $R_{\odot}$ is the Solar radius, σ is the Stefan–Boltzmann constant and T_{eff} is the effective temperature at the surface of the Sun, ∼6000 K. Equating the rate of isotropic re-emission of radiation, $4\pi R^2 T_{\mathrm{g}}^4$, to (2.2.1) gives

$$\frac{(1-A)^2 R_{\odot}^2 T_{\mathrm{eff}}^4}{4R^2} = T_{\mathrm{g}}^4. \quad (2.2.2)$$

Taking $(1-A) \approx 1$, for a particle at a distance of 1 au from the Sun, this gives an equilibrium temperature of around 289 K. Gustafson (1994) states that zodiacal dust colours near 1 au are in the 255–300 K range, with colour features calibrated with 10- and 20-μm silicate emissions.

2.3 The Mie-scattering region

For particles with radii comparable to the wavelengths of the incident radiation, evaluating Q_{abs} is complicated by scattering effects. Accurately determining the amount of radiation scattered and absorbed by a particle of arbitrary size and composition is a problem in classical electromagnetic theory. Independent solutions were obtained by Mie (1908) and Debye (1909) by solving Maxwell's equations for a plane-polarized electromagnetic wave incident on a sphere with appropriate boundary conditions. By considering the fraction of incident energy absorbed relative to that which is scattered by the sphere, Q_{abs} can be found.

By making use of the recurrence relations for Riccati–Bessel functions, values of Q_{abs} are obtained for a grain of a given radius and composition (optical constants). These are then used together with the Planck spectrum in the radiation balance equation (2.1.3) to find the equilibrium particle temperature. Small particles are less efficient at emitting infrared radiation than they are at absorbing visible radiation, so such particles will in general be expected to have higher equilibrium temperatures than larger ones. Q_{abs} is also a function of the real and imaginary parts of the refractive index.

2.4 The asymptotic limit

For particles with radii satisfying the condition $2\pi a \ll \lambda$, Q_{abs} can be approximated using the asymptotic approximation (Van de Hurst 1957; Wickramasinghe 1972):

$$Q_{\mathrm{abs}} \approx -\frac{8\pi a}{\lambda}\,\mathrm{Im}\left(\frac{m^2-1}{m^2+2}\right). \quad (2.4.1)$$

The complex refractive index in equation (2.4.1) is given by

$$m = n - \mathrm{i}k, \quad (2.4.2)$$

where n and k are respectively the ordinary refractive and absorptive index. For many real substances n and k are functions of both wavelength and temperature. Equation (2.4.2) implies that (2.4.1) can be written in terms of n and k:

$$Q_{\mathrm{abs}} \approx \frac{48\pi a}{\lambda}\left[\frac{nk}{(2+n^2-k^2)^2+4n^2k^2}\right]. \quad (2.4.3)$$

Assuming that

$$M = \left[\frac{nk}{(2+n^2-k^2)^2+4n^2k^2}\right]$$

is wavelength- and temperature-independent and inserting (2.4.3) into the energy balance equation (2.1.3), analytical integration yields

$$T_{\mathrm{g}}^5 = \frac{1}{4}W\frac{M(\lambda_{\mathrm{vis}}, T_{\odot})}{M(\lambda_{\mathrm{IR}}, T_{\mathrm{g}})}T_{\odot}^5, \quad (2.4.4)$$

assuming that the effective absorption and re-emission wavelengths are large compared with $2\pi a$.

Notice now that the temperature scales as $W^{1/5}$ rather than the $W^{1/4}$ appropriate for the blackbody approximation.

In reality the refractive index is highly dependent on the composition of the sphere, different materials having very different n and k values. Here we consider three cases:

(i) grains composed of ideal greybody-type material;
(ii) dielectric grains;
(iii) organic grains.

In all instances we assume that the grains are homogeneous. If they were composed of a mixture of materials, the overall refractive index could be considered as a volume-weighted average of the different materials within the grain (Hoyle & Wickramasinghe 1979). More complicated procedures such as the Mawell–Garnett mixing rule for spherical inclusions only make a difference for large values of the imaginary part of the refractive index near the peak of the Planck spectrum (Bohren & Wickramasinghe 1977), and will not be considered in the present discussion.

For the above three classes of grain material we will assume a refractive index $m = 1.4 - \mathrm{i}k$. The value $\mathrm{Re}(m) = 1.4$ corresponds to a compact material such has been used to explain polarization of scattered radiation from comets (Mukai 1986).

For an ideal greybody, the refractive index is independent of wavelength. Gustafson (1994) used a value of $m = 1.4 - 0.1\mathrm{i}$. As the value of m is the same in both emission and absorption, (2.4.4) reduces to

$$T_{\mathrm{g}}^5 = \frac{1}{4}WT_{\odot}^5 \quad (2.4.5)$$

in the approximation of grain radii small compared with $\lambda/2\pi$ at all relevant wavelengths. This gives an equilibrium temperature of 530 K.

Ideal, non-conducting dielectric grains have $m \in \mathrm{Re}^+$ and $Q_{\mathrm{abs}} = 0$. For practical purposes dielectric grains can be assumed to have very small values of Im(m). Crystalline silicates such as olivine are a good approximation to a perfect dielectric material. Ossenkopf et al. (1992) determined absorption peaks in the visual/ultraviolet and infrared for such a silicate material. Taking a peak value of m in the visible to be $m = 1.81 - 0.01\mathrm{i}$ and an absorption peak in the infrared to be $m = 1.78 - 0.82\mathrm{i}$, representative of pure silicates, (2.4.4) gives an equilibrium temperature of 250 K, about 280 K lower than for the ideal greybody material.

Low values of Im(m) at visible wavelengths and high values or high resonances at the infrared wavelengths mean that small silicate materials have lower equilibrium temperatures at a solar distance of 1 au than larger greybody materials. Water-ice also exhibits low Im(m) values in the visible spectrum and relatively high values in the infrared. This gives it very low equilibrium temperatures at a distance of 1 au. However, Gustafson (1994) has shown that the inclusion of even a small amount, ∼1 per cent by volume, of contaminate brings the equilibrium temperature close to the blackbody temperature.

When considering the thermal effects on grains released in the coma of P/Halley, Wallis, Rabilizirov & Wickramasinghe (1987) compiled a table for the complex refractive indices of organic grains (see Table 1). They employed a model that used $m = 1.4 - \mathrm{i}k$, with the values of $k(\lambda)$ determined by experimental results for biological organic material in the ultraviolet, visible and infrared.

Most solar radiation is emitted at 0.6 μm; assuming a linear dependence between the experimental points in Table 1, this gives a refractive index of $m = 1.4 - 0.08\mathrm{i}$. Taking the refractive index averaged over the infrared region to be $m = 1.4 - 0.1530\mathrm{i}$, equation (2.4.4) gives an equilibrium temperature for 0.01-μm grains of around 505 K. However, resonances in O–H, C–H and C=C organic bonds suggest that the bulk of the infrared emission would occur at ∼10 μm. Taking the refractive index over the whole infrared region to be essentially that at 10 μm gives a substantially lower equilibrium temperature of 354 K.

Interplanetary dust particles (IDPs) recovered from the Earth's upper atmosphere show the majority of ten-micron-sized particles to be made of fluffy, aggregate material (Brownlee 1978; Wickramasinghe et al. 2002). The refractive indices used above assumed compact spheres composed of a homogeneous medium. Lower values of $\mathrm{Re}(m) \leqslant 1.2$ would provide a simulation for porous grains (Wallis et al. 1987). In the limit $n \sim 1$ and $k \ll 1$, $M \approx k$. Therefore equation (2.4.4) reduces to

$$T_{\mathrm{g}}^5 = \frac{1}{4} W \frac{k_{\mathrm{vis}}}{k_{\mathrm{IR}}}, T_{\odot}^5$$

so we can conclude that the above results are not sensitive to the detailed grain construction for the case of grains with even a modest degree of porosity.

Table 1. Complex refractive index of model organic grains (Wallis et al. 1987).

λ (μm)	K	λ (μm)	K
0.21	0.08	1.05	0.0019
0.23	0.077	2.05	0.0037
0.25	0.375	3.05	0.035
0.35	0.075	4.05	0.015
0.45	0.19	5.05	0.018
0.55	0.01	6.05	0.10
0.65	0.156	7.05	0.06
0.75	0.0014	8.05	0.08
0.85	0.0015	9.05	0.125
0.95	0.0017	10.05	0.94

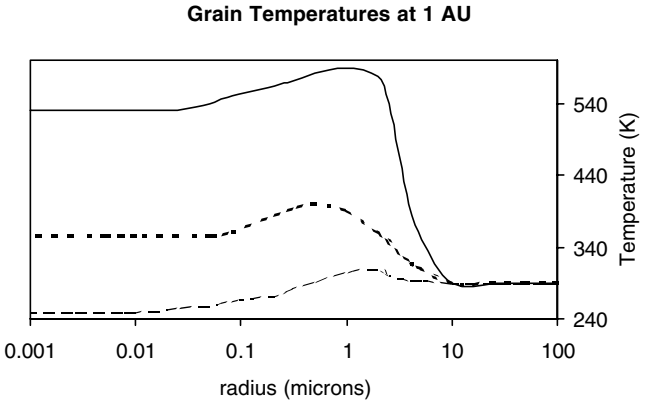

Figure 1. Equilibrium grain temperatures at 1 au from the Sun. The solid line represents grains composed of an idealized greybody material, $m = 1.4 - 0.1\mathrm{i}$. The dashed line is for grains made from a dielectric material, and the middle line is for grains composed of an organic material with refractive indices modelled from Table 1.

2.5 Grain sublimation

The equilibrium grain temperatures at a distance of 1 au from the Sun for different particle radii and materials are summarized in Fig. 1. Ideal greybody grains smaller than 10 μm have higher equilibrium temperatures than larger grains, as they are unable to emit sufficient energy at lower temperatures. For a fixed grain composition the smallest sub-micron grains are at lower equilibrium temperatures than grains with radii of around 1 μm, because the smaller grains are less efficient emitters of infrared wavelengths which are of the same order as the grain radii.

For real grain materials (as opposed to ideal greybody grains), equilibrium grain temperatures are dependent on the composition as well as the grain radius. Organic particles, which are more likely to be found in IDPs than idealized greybody particles (Hoyle & Wickramasinghe 1999), are typically around 280 K, cooler than idealized greybody grains, for particle radii $\leqslant$1 μm. This is because organic molecules tend to have low absorption values in the visible wavelengths and high absorption resonances due to C–H, O–H and C=C bond stretching.

For grains with equilibrium temperatures >300 K and volatile icy composition, energy is lost from the grain by sublimation as well as by radiation emission. To allow for this the energy balance equation (2.1.3) needs an additional term on the right-hand side. If the grain has a mass m and H is the enthalpy of phase change, then (2.1.3) becomes

$$W \int_{\lambda} \mathrm{d}\lambda Q_{\mathrm{abs}}(\lambda, a) B(\lambda, T_{\odot}) = 4 \int_{\lambda} \mathrm{d}\lambda Q_{\mathrm{abs}}(\lambda, a) B(\lambda, T_{\mathrm{g}}) + \frac{1}{4\pi a^2} H \frac{\mathrm{d}m}{\mathrm{d}t}. \quad (2.5.1)$$

This assumes that H is the enthalpy change for both sublimation and vaporization, such that if the melting temperature of the grain is $T_{\rm m}$,

$$H = \begin{cases} H_{\rm s} & T < T_{\rm m} \\ H_{\rm s} + H_{\rm v} & T \geqslant T_{\rm m}. \end{cases}$$

For a spherical grain of radius a and density ρ, the mass lost per unit time $\mathrm{d}m/\mathrm{d}t$ can be written as

$$\frac{\mathrm{d}m}{\mathrm{d}t} = 4\pi a^2 \frac{\mathrm{d}a}{\mathrm{d}t}. \tag{2.5.2}$$

Wallis et al. (1987) calculated the rate of change of energy per surface area using the expression

$$\frac{\mathrm{d}a}{\mathrm{d}t} = -\frac{P(T)}{\rho}\left(\frac{\mu}{2R_{\rm gas}T}\right)^{1/2}, \tag{2.5.3}$$

where $R_{\rm gas}$ is the universal gas constant $R_{\rm gas} = 8.314$ J g mol^{-1} K^{-1}, and μ is the molecular weight of the evaporating material. The pressure $P(T)$ is calculated using the Clausius–Clapeyron equation

$$P(T) = P_{\rm l} \exp\left[\frac{H}{R_{\rm gas}}\left(\frac{1}{T_{\rm l}} - \frac{1}{T}\right)\right]. \tag{2.5.4}$$

P is a reference vapour pressure; normally $P_{\rm l} = 1$ torr. Equation (2.5.4) is valid only in the region where the pressure is sufficiently low, as is the case for typical sublimation grain pressures.

Defining the grain half-lifetime τ as the time for the grain radius to decrease to half its original value, we have

$$\tau = \frac{1}{2}\left(\frac{a}{|\dot{a}|}\right), \tag{2.5.5}$$

where $\dot{a} = \mathrm{d}a/\mathrm{d}t$, calculated from (2.5.3) and (2.5.4).

Wallis et al. (1987) calculated lifetimes of grains comprised of ice with graphite impurities, evaporated from the coma of P/Halley at times $\tau < 100$ *s*, the precise value being dependent on impuity content. Sub-micron grains with radii of 0.3 and 0.1 μm composed of the same material had lower half-lifetimes of $\tau \leqslant 10$ s at the same solar distance of 1 au.

2.6 Conclusion

The temperatures greater than 500 K calculated for small ideal greybody grains suggest that such small particles with radii less than 10 μm if they are made of volatile ices or organics are unlikely to survive in free space at solar distances of 1 au or less. Larger greybody spheres (∼100 μm) or smaller particles composed of volatile organics and ices with equilibrium temperatures of around 350 K are also unlikely to survive at these distances.

Volatile, organic material contained within heterogeneous spheres with radii of $\geqslant$10 μm, composed of a mixture of ice, carbonaceous and organic matter have equilibrium temperatures of ∼290 K and are able to survive at solar distances of 1au. So too are those non-volatile organic spheres with radii of 0.01 μm that have $Q_{\rm abs}({\rm vis}) < Q_{\rm abs}({\rm IR})$. The next section of this paper examines the heating effects on these particles as they interact with the Earth's upper atmosphere.

3 MICROMETEOROID HEATING BY THE EARTH'S ATMOSPHERE

During its passage through the Earth's atmosphere, a micron-sized meteoroid is subjected to bombardment by the air molecules within the atmosphere. Earlier work (Coulson 2002) has described the process by which the meteoroid velocity is attenuated by momentum transfer to the air molecules. In this section the thermal effects of the interaction between the meteoroid and the air molecules are considered.

Many authors (Fraundorf 1980; Nicol et al. 1985; Love & Brownlee 1991) have described the heating effects of the atmosphere on small meteoroids. In general, these authors confined their treatment to meteoroids with radii greater than 10 μm and considered them to behave as ideal black- or greybodies with an emissivity ≈1. As seen in Section 2, radiation scattering affects the absorption and emission efficiencies for particles with radii <10 μm. As meteoroids collected at heights of around 40 km have radii of under 10 μm (Wickramasinghe et al. 2002), it is worth considering in detail the radiative interactions between these particles and the Earth's atmosphere.

3.1 Atmospheric heating

The velocity profile of a micron-sized meteoroid, entering the upper atmosphere with hypervelocity speed U_0 and at an angle θ to the downward vertical, is given by (Coulson 2002)

$$U(x) = U_0 \exp\left(-6\frac{H\rho_0 \sec\theta}{a\rho_{\rm m}}\,\mathrm{e}^{-x\cos\theta/H}\right), \tag{3.1.1}$$

where x is the distance travelled through the atmosphere relative to a fixed point on the surface of the Earth, and $\rho_{\rm m}$ is its density. It is assumed that the density of the Earth's atmosphere varies exponentially with altitude (Allen 1973):

$$\rho_{\rm air} = \rho_0\,\mathrm{e}^{-x\cos\theta/H}$$

for some suitable scaleheight H.

When air molecules strike the surface of a hypervelocity meteoroid, it is possible for molecules on the meteoroid to be sputtered off the surface. The momentum transfer from these sputtered particles increases the effectiveness of the atmosphere in decelerating the meteoroid. If the impinging air molecules sputter off meteoroid particles with a momentum enhancement factor of k, the velocity profile is now

$$U(x) = U_0 \exp\left[-6(k+1)\frac{H\rho_0 \sec\theta}{a\rho_{\rm m}}\mathrm{e}^{-x\cos\theta/H}\right]. \tag{3.1.2}$$

A meteoroid of radius a, travelling with velocity U, is bombarded by air molecules at a rate $\pi a^2\rho_{\rm air}U$. This mass of air imparts its kinetic energy $\frac{1}{2}\pi a^2\rho_{\rm air}U^3$ to the meteoroid. Combining the effects of kinetic energy transfer with the radiative heating mechanism discussed in Section 2 gives a thermal balance equation

$$\frac{\Lambda}{2}\pi a^2\rho_{\rm air}U^3 + \pi a^2 W\int_\lambda \mathrm{d}\lambda\, Q_{\rm abs}(a,\lambda)B(\lambda,T_*) = 4\pi a^2\int_\lambda \mathrm{d}\lambda\, Q_{\rm abs}(a,\lambda)B(\lambda,T_{\rm g}) + \frac{4}{3}\pi a^3\rho_{\rm m}c\frac{\mathrm{d}T_{\rm g}}{\mathrm{d}t}. \tag{3.1.3}$$

On the left-hand side, Λ is the heat transfer coefficient between the air molecules and the meteoroid, and T_* is the effective temperature of the Earth's atmosphere.

The final term on the right-hand side represents the heat conducted through the meteoroid with specific heat capacity c. Heat conduction is an important mechanism to consider in the case of larger meteoroids, where temperature gradients $\mathrm{d}T_\mathrm{g}/\mathrm{d}t$ give rise to different degrees of heating at different points within the body. For small meteoroid particles with radii of around 10 μm or less, heat conduction is normally insignificant, as the temperature gradient across the body is small enough for it to be considered isothermal. The Biot number (Bi) is used to estimate the effects of conduction:

$$Bi = \frac{hL}{K},$$

where L is the scalelength of the body, h the heat transfer coefficient through the body and K the thermal conductivity. In general, a body can be considered isothermal if $Bi < 0.1$ (Kakaç & Yener 1985). Using Biot numbers as a guide, Love & Brownlee (1991) considered that micrometeoroids begin to exhibit thermal gradients near their peak temperatures at radii greater than 500 μm. As the particles considered here will be at least an order of magnitude smaller, the effects of heat conduction will be ignored and the meteoroids treated as isothermal.

When modelling the temperature profiles of meteoroids as they descend through the atmosphere, most authors ignore the effects of radiative heating on the meteoroid. In the collision-free regime in the Earth's upper atmosphere, the bulk of radiative heating comes from the solar radiation field, as the atmosphere is in thermally decoupled from the meteoroid. Lower down in the Earth's atmosphere, the meteoroid will absorb radiation from the atmosphere, which can be modelled as a blackbody with the effective temperature of the local atmosphere. For hypervelocity meteoroids, the dominant heating effect comes from the kinetic energy of the incident air molecules and so the radiative effects of heating can be ignored, removing the second term on the left-hand side of (3.1.3). It will be assumed that the particles have initial temperatures equal to their equilibrium temperatures at a solar distance of 1 au, given in Section 2.

On the right-hand side of (3.1.3), the emission of radiation by the particle is the major source of cooling. As with the description of grain temperatures in Section 2, the size of the particle affects the efficiency at which energy is re-radiated by the particle. As above, three separate cases will be considered: the blackbody approximation for particles with $a \geqslant 10$ μm, the Mie scattering region $0.01 < a < 10$ μm and the asymptotic limit $a \leqslant 0.01$ μm.

3.2 Meteoroids with $a \geqslant 10$ μm

For particle sizes greater than the wavelengths of the absorbed and the emitted radiation, the particle can be considered as a blackbody ($\epsilon = 1$) or a greybody ($\epsilon \leqslant 1$). The amount of energy emitted by the particle varies as T^4 and (3.1.3) becomes

$$\frac{\Lambda}{2}\rho_\mathrm{air}U^3(x) = 4\epsilon\sigma\left(T_\mathrm{g}^4 - T_\mathrm{e}^4\right), \tag{3.2.1}$$

where $\sigma = 5.67 \times 10^{-8}$ J m^{-2} K^{-4} s^{-1} is the Stefan–Boltzmann constant and T_e is the equilibrium grain temperature. Substituting (3.1.1) into (3.2.1) along with the expression for the air density ρ_air gives

$$T_\mathrm{g}^4 = T_\mathrm{e}^4 + \frac{\rho_0\Lambda}{8\epsilon\sigma}U_0^3\left[\exp\left(-18\frac{H\rho_0\sec\theta}{a\rho_\mathrm{m}}\,\mathrm{e}^{-x\cos\theta/H}\right)\right]. \tag{3.2.2}$$

The profile of temperature versus altitude is shown in Fig. 2. A 100-μm meteoroid particle with an initial velocity of 12 km s^{-1} attains a maximum temperature of just above 1500 K, at an altitude

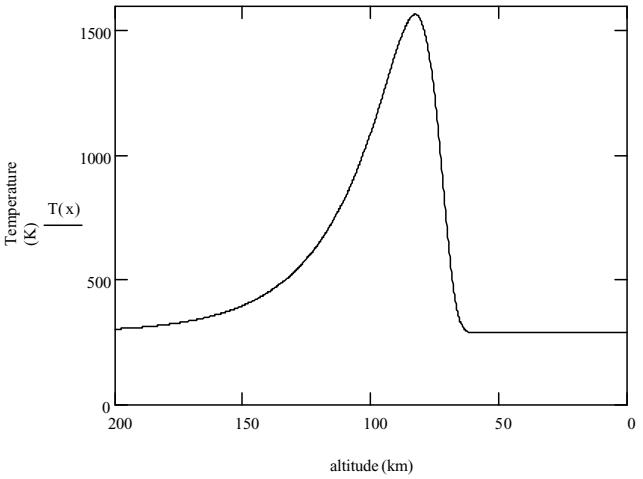

Figure 2. The temperature profile for a 100-μm particle with a density of 3 g cm^{-3} and an initial velocity of 12 km s^{-1}, and an entry angle of 45°.

of 90 km above the Earth. Love & Brownlee (1991) derived similar results for a particle with similar characteristics.

Equation (3.2.2) tends to overestimate the maximum temperature attained by the meteoroid, as it does not allow for the energy lost during evaporation and sublimation. The energy lost as a result of evaporation and sublimation can be a significant fraction of the total energy, around 10 per cent for a 12 km s^{-1} stone meteoroid (Love & Brownlee 1991). For meteoroids composed of organic and more volatile materials than stone, the fraction of energy lost because of sublimation is less. Evaporation is a function of temperature and is greatest around the point of maximum heating, so the cooling effects of ablation can often mitigate the maximum temperature of the meteoroid.

Particles with hypervelocity speeds also experience mass loss because of the effects of sputtering. For a particle slowed by sputtering, the velocity profile falls off more rapidly than for the unsputtered case and so the amount of kinetic energy transferred from the air molecules is less. Energy is also carried away from the meteoroid in the form of the kinetic energy of the sputtered particles.

In the case of a meteoroid air-braked by sputtering, the velocity equation to be substituted into (3.2.1) is (3.1.2). Additional terms must be included to account for energy lost as the kinetic particles, and for the energy required to overcome the binding of surface molecules to the meteoroid. In general, this is small compared with the fraction of energy removed as kinetic energy, and thus can be ignored.

The kinetic energy of the sputtered particles is equal to

$$\frac{1}{2}\pi a^2\rho_\mathrm{air}\int_0^\infty \mathrm{d}v\, vf(v)\int_0^\infty \mathrm{d}v'\, v'^2 g(v'), \tag{3.2.3}$$

where $f(v)$ is the velocity distribution of the impinging air molecules and $g(v)$ is the velocity distribution for the sputtered molecules. Adding this term on to the right-hand side of equation (3.2.1) gives

$$T_\mathrm{g}^4 = T_\mathrm{e}^4 + \frac{\rho_\mathrm{air}}{8\epsilon\sigma}\left[\Lambda U^3(x) - \int_0^\infty \mathrm{d}v\, vf(v)\int_0^\infty \mathrm{d}v'\, v'^2 g(v')\right]. \tag{3.2.4}$$

In the hypervelocity limit, to a first approximation, (3.2.3) reduces to

$$\frac{1}{2}\pi a^2\rho_\mathrm{air}\Gamma U^3(x),$$

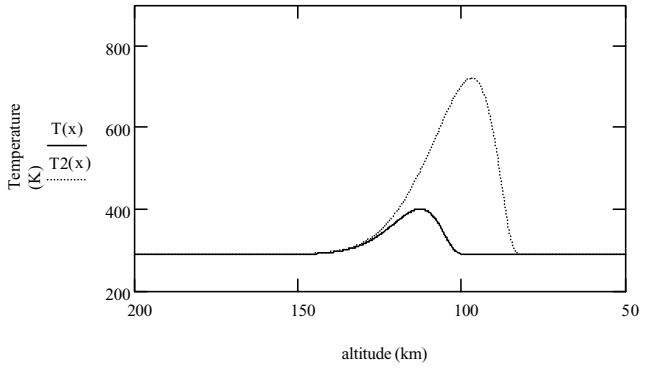

Figure 3. Temperature profiles for identical 10-μm particles with an initial velocity of 12 km s^{-1} and a density of 3 g cm^{-3}. The dotted curve is for a particle slowed by specular reflection of air molecules described by equation (3.2.1), and the solid curve is for a particle slowed by sputtering, with a sputtering coefficient $S = 0.9$ and a momentum enhancement $k = 1.5$.

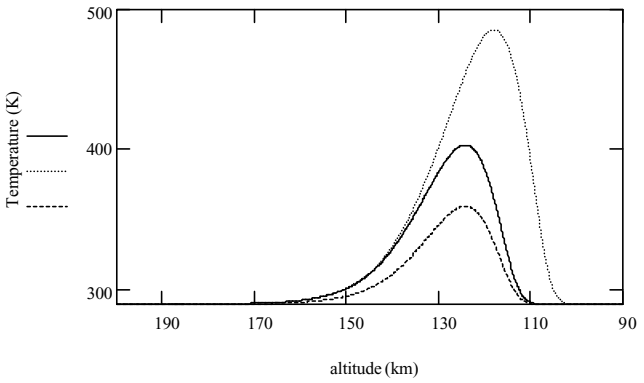

Figure 4. Temperature profiles for 10-μm particles with a density of 0.6 g cm^{-3}, an initial velocity of 12 km s^{-1} and an entry angle of 45°. The highest curve is for a particle slowed by specular reflection of air molecules. The middle curve is for an identical particle slowed by sputtering, with a sputtering coefficient of 0.99. The lowest curve shows a particle slowed by sputtering, with a relatively low sputtering coefficient of 0.5.

where Γ is the fraction of energy carried off as kinetic energy by the sputtered particles. Defining S, the sputtering coefficient, such that

$$S = 1 - \Gamma,$$

(3.2.4) becomes

$$T_g^4 = T_e^4 + \frac{\rho_{air}}{8\epsilon\sigma} SU^3(x). \tag{3.2.5}$$

Substituting the exponential expression for the air density and the sputtering velocity profile (3.1.2) into (3.2.5),

$$T_g^4 = T_e^4 + \frac{\rho_0 e^{-x\cos\theta/H}}{8\epsilon\sigma} \Lambda S U_0^3 \times \left\{ \exp\left[-18(k+1)\frac{H\rho_0 \sec\theta}{a\rho_m} e^{-x\cos\theta/H} \right] \right\}. \tag{3.2.6}$$

Fig. 3 shows the difference in maximum temperature when a meteoroid is slowed by sputtering rather than by specular reflection of the impinging air molecules.

The meteoroid slowed by specular reflections attained a maximum temperature almost twice as great as the meteoroid retarded by sputtering. In this case, the meteoroids considered had a relatively high density, $\rho_m = 3.0$ g cm^{-3}; this density can be considered typical for stone meteoroids. As stone meteoroids contain a relatively low amount of volatile material, the momentum enhancement, k, was assumed to have a low value of 1.5 and the proportion of energy removed as the kinetic energy of the sputtered particles was 0.1.

Cometary particles are assumed to be a significant component of the IDP flux into the Earth, although the precise fraction is as yet difficult to estimate (Jeffers et al. 2001; Kortenkamp & Dermot 1998). If the cometary component is similar to the particle aggregate recently collected in the stratosphere (Harris et al. 2002), such particles would have an average density of ∼0.6 g cm^{-3} and an average radius of ∼10 μm. The temperature profiles for such a 10-μm meteoroid composed of a cometry material are shown in Fig. 4.

Meteoroids composed of cometary material attain lower temperatures than the denser stone material meteoroids. The middle curve shown in Fig. 4 is for a meteoroid with a sputtering coefficient $S = 0.99$; this implies that only a fraction of 0.01 of the energy was carried off in the kinetic energy of the sputtered particles. The lowest curve is for a sputtering coefficient $S = 0.5$. The difference in the maximum temperature attained by these two meteoroids is ∼50 K; this illustrates the sensitivity of S to the temperature profile of the meteoroid. The wide range in the temperature response to variations of the parameter S evident in Fig. 4 highlights the difficulty of predicting a precise temperature profile for incoming meteoroids. The actual situation in respect of sputtering is contingent on several factors such as particle size, composition, shape and porosity that remain uncertain. Sputtering yields in laboratory studies have been found to be sensitive to composition and impact energies, with yields at energies ⩽10 eV being negligible in many cases (Jurac et al. 1998). The sputtering model considered here defined by the velocity profile (3.1.2) may require significant modification for the case of highly fluffy and porous meteoroids. In such a case, sputtered ions will be mostly trapped within the porous matrix and thus will not contribute to momentum transfer. Therefore porous grains may be expected to achieve higher temperature peaks, as in fact indicated by erasures of cosmic ray tracks and dehydration of hydrated silicates in Brownlee particles (Klock et al. 1994).

3.3 Meteoroids with $a \leqslant 1$ μm

For particles with radii less than 10 μm the effects of radiation scattering alter the energy re-radiated term on the right-hand side of (3.1.3). In the asymptotic limit

$$Q_{abs} \approx -\frac{8\pi a}{\lambda} \mathrm{Im}\left(\frac{m^2-1}{m^2+2}\right),$$

assuming that the real and imaginary values of the refractive index are independent of temperature and wavelength. Integrating this approximation for Q_{abs} with the Planck spectrum over the entire range of λ gives

$$\int_\lambda d\lambda Q_{abs}(a,\lambda) B(\lambda, T_g) \approx 9504\pi^2 a \frac{k_B^5}{h^4 c^4} \times \left[\frac{nk}{(2+n^2-k^2)^2+4n^2k^2}\right] T_g^5, \tag{3.3.1}$$

where n and k are, respectively, the real and imaginary parts of the refractive index, $k_B = 1.38 \times 10^{-23}$ J K^{-1} is the Boltzmann constant, h is Planck's constant and c is the speed of light. So the rate at which radiation emitted is now proportional to T_g^5, as found in Section 2.

Substituting (3.3.1) into (3.1.3) gives

$$T_g^5 = \Lambda \frac{\rho_{air}}{76\,032\pi^2 a} \frac{h^4 c^4}{k_B^5} \left[\frac{nk}{(2+n^2-k^2)^2+4n^2k^2}\right]^{-1} U^3(x), \tag{3.3.2}$$

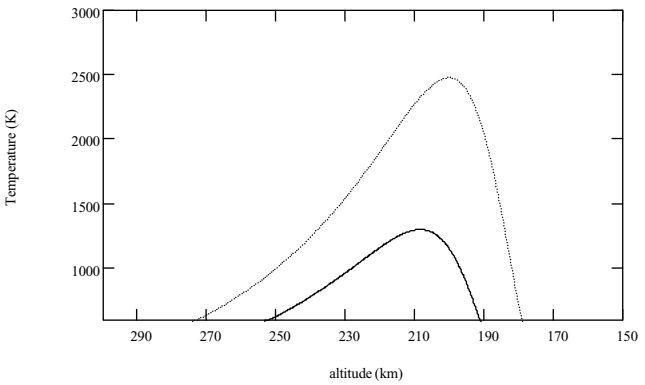

Figure 5. Temperature profiles for 0.1-μm organic particles with a density of 0.6 g cm^{-3}, an initial velocity of 12 km s^{-1} and an entry angle of 45°. The upper curve is for a particle slowed by specular reflection of air molecules, and the lower curve is for a particle air-braked by sputtering, with $S = 0.9$.

where (3.1.1) is used for $U(x)$ if the meteoroid is slowed by specular reflection of the air molecules, and (3.1.2) if the meteoroid is air-braked by a sputtering process. In the case of sputtering, the second term on the right-hand side of (3.3.2) is multiplied by the sputtering coefficient S, to take account of the energy removed as the kinetic energy of the sputtered molecules.

As can be seen from Fig. 5, the 0.1-μm particles reach very high temperatures of over 2500 K for non-sputtered particles and over 1500 K for sputtered particles, very high up in the atmosphere.

4 MICRON-SIZED METEOROID SURVIVAL

The temperature profiles for 10- and 0.1-μm particles are summarized in Figs 4 and 5. In general, particles with radii $a < 1$ μm do not survive the passage through the Earth's atmosphere, as they are unable to radiate heat efficiently at lower temperatures; the temperature rises to the point where the meteoroid is vaporized.

Micrometeoroids with radii $a = 10$ μm or greater do survive the passage through the Earth's atmosphere. They are sufficiently small to be slowed down from their entry velocities before they reach the denser parts of the atmosphere (∼80 Km above the Earth) where most meteoroids with radii 1 mm $< a <$ 1 cm are burned up. Meteoroids with a surface layer that is sputtered off by air molecules are slowed more gently than meteoroids retarded by specular reflection and so they attain lower maximum temperatures.

The meteoroids are only heated to their maximum temperatures above their equilibrium temperatures for a short period, of the order of seconds. It is possible for organic materials to survive this process of flash heating relatively undamaged. Even clumps of viable bacteria – if they are introduced as micron-sized meteoroids – could survive flash heating in the atmosphere. For example, Al-Muffi, Hoyle & Wickramasinghe (1999) subjected a culture of *E. coli* bacteria to brief exposures of heat for durations of between 30 and 60 s. They discovered that the *E. coli* remained a viable culture after stepwise heating to temperatures from 540 to 1120 K. Section 3 suggests that the conditions experienced by organic material in the form of 10-μm-sized particles are not as severe, as those survived by the *E. coli* involved higher temperatures and a greater duration of heating.

4.1 Micrometeoroids settling through the atmosphere

On entering the Earth's atmosphere, 10-μm-sized particles are rapidly slowed from their initial entry speeds >10 Km s^{-1} by collisions with air molecules. As can be seen from Section 3, these particles are slowed from hypervelocity speeds to rest at altitudes ∼100 Km. These particles then slowly descend through the atmosphere with settling speeds of the order of cm s^{-1} (Kasten 1968). Treating the particle as isothermal and applying the energy balance equation from (3.1.3) gives

$$\frac{\Lambda}{2}\pi a^2 \rho_{\rm air} U^3 + \pi a^2 W \int_\lambda {\rm d}\lambda\, Q_{\rm abs}(a,\lambda) B(\lambda, T_*) = 4\pi a^2 \int_\lambda {\rm d}\lambda\, Q_{\rm abs}(a,\lambda) B(\lambda, T_{\rm g}). \quad (4.4.1)$$

Equation (4.1.1.) looks like this because the particle speed, U, is equal to the settling velocity. This implies that the heating effect of the air molecules, proportional to U^3, is very small compared with the effects of radiation absorption. Ignoring the heating of the meteoroid by air molecules, (4.1.1) becomes

$$\pi a^2 W \int_\lambda {\rm d}\lambda\, Q_{\rm abs}(a,\lambda) B(\lambda, T_*) = 4\pi a^2 \int_\lambda {\rm d}\lambda\, Q_{\rm abs}(a,\lambda) B(\lambda, T_{\rm g}). \quad (4.1.2)$$

Equation (4.1.2) is identical to the energy balance equation (2.1.3) for particles in free space. At an altitude of 90 km above the surface of the Earth, $W \approx 0.97$, using which the temperature of a given function $Q_{\rm abs}(a, \lambda)$ can be calculated from equation 4.1.2.

Following mass lost because of the effects of sputtering and sublimation, it is reasonable to assume that a hypervelocity meteoroid with an initial radius of 10 μm is reduced. The extent of this reduction varies enormously, depending on the entry velocity, angle of incidence and on the size and composition of the meteoroid. In an extreme case, one might expect an effective radius of ∼1 μm by the time the particle has reached its settling velocity. For a blackbody at 300 K, the maximum intensity occurs at a wavelength $\lambda \approx 9$ μm. For a particle with an effective radius of ∼1 μm, the particle can be considered to be absorbing in the asymptotic limit $2\pi a \ll \lambda$ and the particle temperature can be evaluated using (2.4.4):

$$T_{\rm g}^5 = \frac{1}{4} W \frac{M(\lambda_{\rm IR}, T_{\rm E})}{M(\lambda_{\rm IR}, T_{\rm g})} T_{\rm E}^5, \quad (4.1.3)$$

where $T_{\rm E}$ is the effective temperature of the Earth, ∼300 K. An ideal greybody, with a refractive index independent of λ, has an equilibrium temperature of ∼298 K at an altitude of 90 km. An organic material has a lower equilibrium temperature, ∼200 K, at the same altitude. From Table 1 it can be seen that Im(m) is greater at 10 μm than for shorter infrared wavelengths. So organic particles are more efficient at re-emitting radiation than absorbing it at these wavelengths, compared with an idealized greybody material.

4.2 Conclusion

The meteoroid temperatures calculated above all assumed an entry angle of 45°; at shallower entry angles the temperatures attained are lower. For a meteoroid entering the Earth's atmosphere at an angle almost parallel to the local horizon, with a speed greater than the Earth's escape velocity, it is possible for it to leave the atmosphere. There is a high possibility that such a meteoroid can re-enter the atmosphere at a later time, with a lower entry speed. This process can be repeated a number of times; in this manner it is possible for

some meteoroids to enter the atmosphere for a final time with low velocities. Meteoroid particles entering the atmosphere in this way are subjected to less atmospheric heating than the meteoroids that enter at higher velocities discussed above.

The results from Section 4.1 illustrate the ability of micron-sized meteoroids composed of organic materials to survive settling through the atmosphere at low speeds. If these particles can survive the initial deceleration process without becoming ablated in the upper atmosphere, they will reach the surface of the Earth after a period of the order of years. Mechanisms such as sputtering and multiple atmospheric entry help to reduce the temperatures attained by meteoroid particles in the upper atmosphere. This widens the class of organic meteoroids able to reach the Earth.

ACKNOWLEDGMENTS

We are grateful to Prof D. E. Brownlee for his helpful suggestions and comments.

REFERENCES

Allen C. W., 2000, Astrophysical Quantities. Athlone Press, London
Al-Mufti S., Hoyle F., Wickramasinghe N. C., 1999, Ap&SS, 268, 51
Bohren C. F., Huffman D. R., 1983, Absorption and Scattering of Light by Small Particles. Wiley, New York
Bohren C. F., Wickramasinghe N. C., 1977, Ap&SS, 50, 461
Bronshten V. A., 1983, Physics of Meteoroidic Phenomena. Reidel, Dordrecht
Brownlee D. E., 1978, in McDonnell J. A. M., ed., Cosmic Dust. Wiley, New York
Coulson S. G., 2002, MNRAS, 332, 741
Debye P., 1909, Ann. Physik, 30, 59
Fraundorf P., 1980, Geophys. Res. Lett., 10, 765
GustafsonÅ. S., 1994, Ann. Rev. Earth Planet. Sci., 22, 553
Harris M. J. et al., 2002, in Hoover R. B., Levin G. V., Paepe R. R., Rozanov A. Y., eds, Proc. SPIE Vol. 4495, Instruments, Methods, and Missions for Astrobiology IV. Int. Soc. Opt. Eng., Bellingham, WA, p. 192
Hoyle F., Wickramasinghe N. C., 1979, Ap&SS, 66, 77
Hoyle F., Wickramasinghe N. C., 1999, Ap&SS, 268, 137
Jeffers S. V., Manley S. P., Bailey M. E., Asher D. J., 2001, MNRAS, 327, 126
Jurac S., Johnson R. E., Donn B., 1998, ApJ, 503, 247
Kakaç S., Yener Y., 1985, Heat Conduction. Hemisphere, New York
Kasten F., 1968, J. Appl. Meteoroidol., 7, 944
Klock W. et al., 1994, Lunar Planet. Conf. Abstr., 25, 713
Kortenkamp S. J., Dermot S. F., 1998, Icarus, 135, 469
Kuhrt E., 1984, Icarus, 60, 512
Love S. G., Brownlee D. E., 1991, Icarus, 89, 26
Love S. G., Brownlee D. E., 1993, Sci, 262, 550
Mie G., 1908, Ann. Physik, 25, 377
Mukai T. et al., 1986, A&A, 164, 397
Nicol E. J., Macfarlane J., Hawkes R. L., 1985, Planet. Space Sci., 3, 315
Ossenkopf V., Henning Th., Mathis J. S., 1992, A&A, 261, 567
Van de Hurst, H. C., 1957, Light Scattering by Small Particles. Dover, New York
Wallis M. K., Rabilizirov R., Wickramasinghe N. C., 1987, A&A, 187, 801
Whipple F. L., 1950, Proc. Natl Acad. Sci. Am., 36, 687
Wickramasinghe N. C., 1972, Light Scattering by Small Particles. Wiley, New York
Wickramasinghe N. C., Lloyd D., Wickramasinghe J. T., 2002, in Hoover R. B., Levin G. V., Paepe R. R., Rozanov A. Y., eds, Proc. SPIE Vol. 4495, Instruments, Methods, and Missions for Astrobiology IV. Int. Soc. Opt. Eng., Bellingham, WA, p. 255

This paper has been typeset from a TEX/LATEX file prepared by the author.